Low frequency E-symmetry phonon modes in $LiTaO_3$: a non-linear temporal domain approach

2000 J. Phys.: Condens. Matter 12 7175

(http://iopscience.iop.org/0953-8984/12/32/302)

J. Phys.: Condens. Matter **12** (2000) 7175–7182. Printed in the UK PII: S0953-8984(00)09638-7

Low frequency E-symmetry phonon modes in $LiTaO_3$: a non-linear temporal domain approach

C A Gautier, M Mérian and J Etchepare

Laboratoire d'Optique Appliquée UMR 7639, ENSTA Centre de l'Yvette, 91761 Palaiseau Cédex, France

Received 17 November 1999, in final form 8 May 2000

Abstract. We present a non-linear temporal domain analysis that allows us to choose among previously published attributions of LO and TO E-symmetry phonon modes in the $LiTaO_3$ crystal. The work is based on the fact that an appropriate study of the phonon–polariton regime enables us to reach a better accuracy in the knowledge of the one-phonon dynamics characteristics. The use of a temporal domain four wave mixing technique with ultra-short light pulses is a powerful tool in this respect. Precise examination of the phonon–polariton dispersion gives the $\varepsilon_\perp$ component of the dielectric tensor. Polariton damping leads moreover to appreciation of the strength of the various temporal responses.

Lithium tantalate ($LiTaO_3$) has been the subject of considerable interest over the past decades as a result of its non-linear optical properties, and because of the intense electro-optic effect it exhibits. The relations that exist between non-linear optical coefficients, IR absorption and Raman scattering efficiencies of LO and TO phonons have therefore motivated general spectroscopic studies [1], and also recording of numerous Raman spectra [2–4]. There has been renewal in interest in these issues due to the development of non-linear spectroscopy. More, using ultra-short laser pulses in a four wave mixing scheme makes it possible to describe low frequency phonon dispersion curves in a rather large extent of phonon wavevector values around the Brillouin zone centre. There, the phonon–polariton regime is of particular interest as low frequency vibrational modes contribute mostly to the magnitude of the dielectric constant in ferroelectric crystals. In this respect, particular attention has been paid on the lowest energy A_1 mode from $LiTaO_3$ [5, 6].

Our work is devoted to the study of E-symmetry phonon–polariton dispersion curves. Previous assignments of the LO–TO frequencies of the E-modes close to the Brillouin zone centre [1, 4] were in conflict, in part because of an inadequate number of measurable peaks, with those predicted by group theory, whatever the actual (C_3, C_{3v} or D_{3v}) symmetry space group of the crystal. The main goal of this contribution consists in the study of the phonon–polariton characteristics, first to enlighten and correct preceding TO–LO attributions, and second to have a direct insight into the contribution from the low frequency phonons to the dielectric constant.

It is well known that using ultra-short temporal pulses allows us to drive coherently any phonon with frequency range within the spectral extent of the pump [7]. The laser used in this study is a colliding pulse mode-locked oscillator connected to a four stage amplifier that delivers 70 fs pulses at 20 Hz centred at 615 nm. Such temporal widths allow us to drive phonons up to $\sim$300 cm^{-1} frequency. The necessary energy density for the pump pulse on the sample is of the order of several GW cm^{-2}; that of the probe pulse is at least ten times smaller. The $LiTaO_3$ sample is an x cut commercial crystal of dimensions $5 \times 5 \times 1$ mm^3 with its optical

0953-8984/00/327175+08$30.00

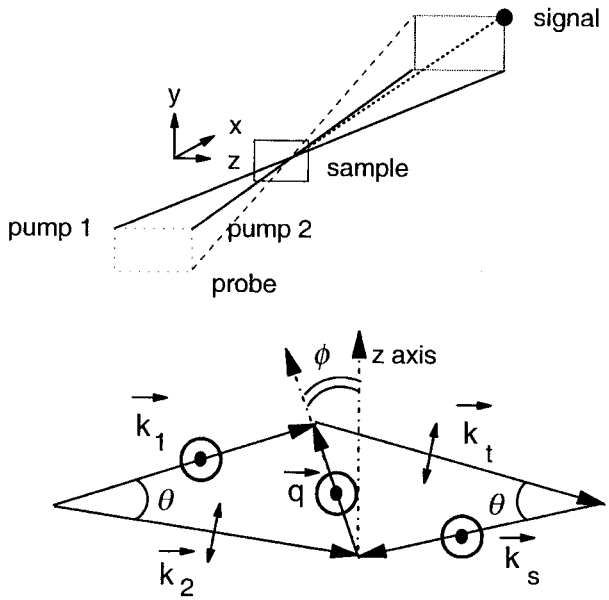

Figure 1. Experimental set-up. Upper part: four beam directions relative to sample axes; lower part: wavevector and beam polarization projections on the (xz) plane.

$c(z)$ axis oriented in the plane of incidence. Experiments are performed at room temperature and the transparency of the crystal at the laser wavelength prevents any lattice heating.

When dealing with solid state excitation, the use of a two pump beam geometry with a crossing angle θ between them permits us to choose the value of the wavevector of interest and therefore describe quite easily the phonon dispersion in the polariton regime. This arrangement is the non-linear temporal analogue to the well known forward Raman scattering experiments in the spectral domain. The Raman tensors associated with active modes of $LiTaO_3$ with C_{3v} symmetry are [4]:

$$A_1 = \begin{bmatrix} a & 0 & 0 \\ 0 & a & 0 \\ 0 & 0 & b \end{bmatrix} \qquad E(x) = \begin{bmatrix} 0 & -c & -d \\ -c & 0 & 0 \\ -d & 0 & 0 \end{bmatrix} \qquad E(y) = \begin{bmatrix} c & 0 & 0 \\ 0 & -c & d \\ 0 & d & 0 \end{bmatrix}.$$

The actually driven phonon symmetry is defined by the pump pulse polarization characteristics. Therefore, selecting exclusively $E(y)$ phonons requires mutually perpendicular polarizations for the pump beams. In the limit where $\theta = 0$, the two fields are held by the same beam, whose polarization is set at 45° from the crystallographic c axis [8].

We present in figure 1 a schematic view of the experiment: the geometrical arrangement of the four beams (pumps, probe and signal), their polarization state and the wavevector direction of the driven phonon–polariton. Excitation (and detection) geometry can be described by a nomenclature analogous to that in use in the literature for Raman scattering experiments, say: $(x + \Delta z)(yz)(x - \Delta z)$. This configuration corresponds to the excitation of ordinary transverse phonon–polaritons [9], for which there is no dispersion that depends on the angle ϕ between the phonon propagation direction and the optical axis. The excited phonon wavevector q can be described by two components, $q_\parallel$ and $q_\perp$, respectively along and perpendicular to the mean direction of propagation of the beams. In the limit where the dispersion of the indices along

the spectral range of the femtosecond pulses is not taken into account [10], their value reads:

$$q_{\parallel} = \omega_L \left\{ \lfloor n_0^2 - \sin^2(\theta/2) \rfloor^{1/2} - \lfloor n_e^2 - \sin^2(\theta/2) \rfloor^{1/2} \right\} \tag{1}$$

$$q_{\perp} = 2\omega_L \sin(\theta/2) \tag{2}$$

where n_0 and n_e are the ordinary and extraordinary refractive indices [11] and ω_L is the central frequency of the laser. Tuning the angle θ from $\sim 4^\circ$ to 0° allows us to describe the dispersive behaviour of the phonons from respectively $q \sim 968\ \mathrm{cm}^{-1}$ to $q = 71.5\ \mathrm{cm}^{-1}$, a value limited by the anisotropy extent of $LiTaO_3$ at the laser wavelength. The efficiency of the non-linear interaction rises its maximum at perfect phase matching between pump, probe and signal beams. Geometrical and polarization characteristics for the probe and signal beam directions are therefore symmetrical to the excitation ones with respect to the (xz) plane.

In the temporal domain, phonon modes may be modelled by damped sinusoids. In the limit where the pump and probe temporal pulses can be approximated by δ functions, it can be shown that the measured signal, the so called quadratic signal, is related to the squared sum of individual response functions:

$$S(q,t) \propto \left[\sum_j A_j \exp\left(-\frac{t}{\tau_j}\right) \sin(\omega_j(q)t) \right]^2 \tag{3}$$

where A_j and $1/\tau_j$ are the amplitude and damping of the jth mode. In the spectral domain, the response function can be written after Barker and Loudon [12] as:

$$R(q,\Omega) = \mathrm{Im}\left[\frac{1}{c^2q^2/\Omega^2 - \varepsilon_{\perp}(\Omega)} \right] \tag{4}$$

where, as we are concerned with ordinary phonons, $\varepsilon_{\perp}(\Omega)$ is the component of the dielectric tensor perpendicular to the optical axis. In the spectral range where the phonons contribute mostly, the dielectric function $\varepsilon_{\perp}(\Omega)$ can be developed as follows:

$$\varepsilon_{\perp}(\Omega) = \varepsilon_{\perp}(\infty)\left[1 + \sum_j \frac{s_j\omega_{TOj}^2}{\omega_{TOj}^2 - \Omega^2 - \mathrm{i}\Omega\gamma_{TOj}} + s' \right]. \tag{5}$$

Here $\varepsilon_{\perp}(\infty)$ is the optical (high frequency) dielectric constant, s_j the oscillator strength from mode j having ω_{TOj} transverse frequency and γ_{TOj} damping, s' depicts the contribution from higher non-driven frequencies. The zeros of the dielectric function provide ω_{LOj} longitudinal frequencies. The dispersion relation reads:

$$c^2q^2/\Omega^2 - \varepsilon_{\perp}(\infty) = \left[1 + \sum_j \frac{s_j\omega_{TOj}^2}{\omega_{TOj}^2 - \Omega^2 - \mathrm{i}\Omega\gamma_{TOj}} + s' \right] = 0. \tag{6}$$

It contains j complex roots ($\Omega = \mathrm{i}\gamma \pm \omega$) for each q value. Experimentally available q values one can reach permit the description of the phonon dispersion in the phonon–polariton regime and, as a consequence, give access to the low frequency dielectric constant.

Figure 2 gathers four theoretical sets of dispersion curves calculated using equation (5). In each set, corresponding respectively to [1] to [4], drawn frequency phonon branches are fitted using ω_{TOj} and ω_{LOj} Raman and/or IR measured values. Thus, for part (a) of figure 2, we have used published oscillator strength values. In contrast, for sets (b) to (d), s_j values were taken as adjustable parameters; confidence in the curvature of these dispersion lines may be therefore quite poor. The calculated dispersion line behaviour allows us first to evidence discrepancies between the various LO–TO assignments. We will demonstrate that an exhaustive measurement of the phonon–polariton frequencies in the high dispersion regime is a unique tool for establishing the various true LO–TO assignments.

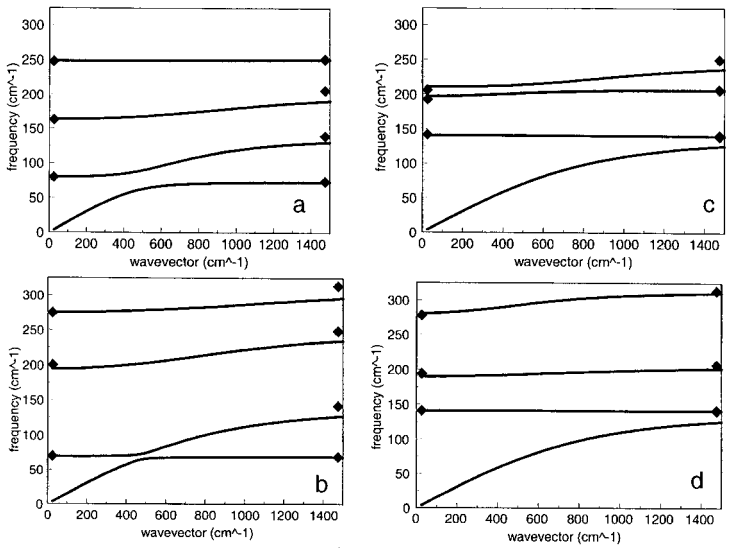

Figure 2. Scheme of the phonon–polariton dispersion curves, as obtained by using equation (5): a corresponds to [1], b to [2], c to [3] and d to [4].

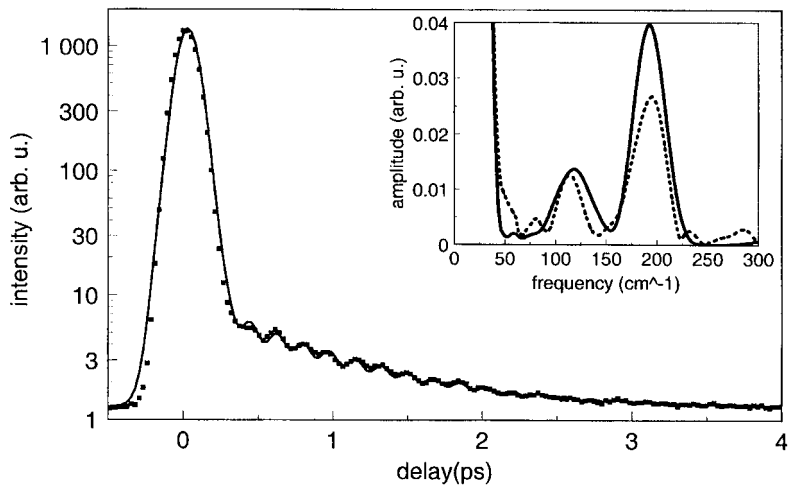

Figure 3. Diffracted signal as a function of the delay between pump and probe pulses; squares correspond to experimental results and lines to fit using equation (2); the inset gives Fourier transforms of the experimental and theoretical signals.

Figure 3 presents the temporal signals that correspond to $\theta = 2.414^\circ$ and therefore $q = 686\ \mathrm{cm}^{-1}$. The strong initial part at vanishing temporal delay between pump and probe pulses corresponds to the electronic response. It is followed by periodic damped oscillations observed for several picoseconds. This is the signature of the different phonon modes. Figure 3 displays also the theoretical response (as derived from equation (2)) that corresponds to the best fit to experiment. As shown in the inset, the Fourier transforms of the temporal curves led to collect combinations of $\omega_j(q)$ phonon frequencies. They have to be attributed to various phonon–polariton frequencies lying on specific dispersion branches. Since linear combinations

Table 1. Frequencies (ν_a, ν_b and ν_c) obtained by Fourier transform of the quadratic signal and their attributions to polariton branches ν_1 and ν_2 or ν_1 to ν_3, with regard to half the angle θ between pump beams and corresponding q values.

$\theta/2$ (°)	q (cm^{-1})	ν_a (cm^{-1}) ($2\nu_1$)	ν_b (cm^{-1}) ($2\nu_2$) or ($2\nu_1$)	ν_c (cm^{-1}) ($\nu_3 - \nu_2$) or ($\nu_2 - \nu_1$)	ν_1 (cm^{-1})	ν_2 (cm^{-1}) or ν_1	ν_3 (cm^{-1}) or ν_2
0.000	71.5	22			11		
0.530	307	100			50		
0.560	325	107			53.5		
0.650	376		145	124		72.5	196.5
0.681	385		157	120		78.5	198.5
0.704	406		151	125		75.5	200.5
0.830	476		158	127		79	206
0.890	512		158	131		79	210
0.925	525		162	129		81	210
1.207	686		184	117		92	209
1.321	753		200	108.5		100	208.5
1.476	841		222	101		111	212
1.700	968		234	98		117	215

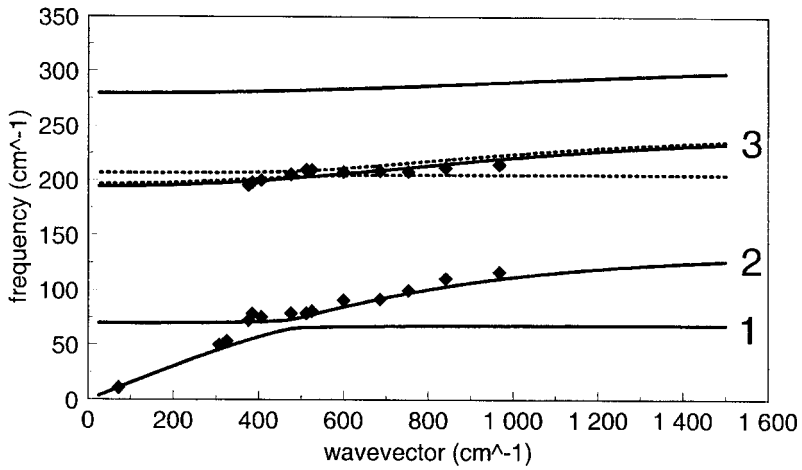

Figure 4. Experimental points (diamonds) and calculated dispersion curves using parameters from table 2; the diamond size recovers estimated wavevector and frequency error bars.

of frequencies that can be temporally resolved by our system are smaller than 250 cm^{-1}, frequencies at our disposal are few with respect to the whole set theoretically involved. The only constraint we used in our choice corresponds to the fact that the dispersion curves do not present any discontinuity. Reported in table 1 are experimental θ angles, associated q values and involved frequencies labelled by an index $i = 1$ to 3 corresponding to the expected dispersion curve. Asking for the existence of two (ν_1 and ν_2) or three (ν_1, ν_2 and ν_3) branches results in a correct fit of both the phonon quadratic signals as derived from equation (2) and the phonon dispersion curves derived from equation (5). Thus the abrupt shift observed in the lowest frequencies near $q = 375$ cm^{-1} can only be modelled by the existence of two E-symmetry branches, the whole set of frequencies leading finally to a three branch model.

Table 2. Calculated oscillator strengths s_j are obtained by using as inputs ν values from table 1 and ν_{TO} (cm^{-1}) and γ_{TO} (cm^{-1}) from [2]; resulting ν_{TO} and ν_{LO} frequencies are in concordance with those from [2]. Numbers in parentheses correspond to a fit that includes a splitting of the third dispersion curve.

[2]			This work		
ν_{TO}	γ_{TO}	ν_{LO}	ν_{TO}	ν_{LO}	s_j
69	21	70	69	69.5	0.4
141	10	200	141	196	4.7
			(206)	(207)	(0.01)
249	7	275	249	275	0.9
316	12	345	314	345	0.7
					0.8 (s')

We have plotted in figure 4 the measured phonon–polariton frequencies with regard with the calculated dispersion curves. Resulting s_j oscillator strengths for the best fit are reported in table 2, together with the data from [2] used in the fitting procedure. The s' contribution from higher branches to the dielectric constant (see equations (4) and (5)) was kept constant. It has been estimated in order that the static dielectric constant, namely $\varepsilon_\perp^0 = \varepsilon_\perp(0)$, as derived from (4) using $\varepsilon_\perp(\infty) = 4.82$, should be in concordance with the clamped experimental value $\varepsilon_\perp^s = 41.0$. The calculated ω_{LOj} values are used as a consistency check.

The results presented in figure 4 call for several comments. Just looking at the behaviour of the lowest phonon–polariton branches, our temporal domain measurements corroborate the attributions proposed by Penna *et al*. A phonon–polariton regime, characterized by a non-linear technique conducted in the temporal domain, gives therefore a conclusive justification to previous attributions based on Raman scattering by oblique phonons [2]. Concerning IR data, calculated strengths remain in qualitative agreement with the pioneer work by Johnston [1]. We explain the non-simultaneous existence of experimental points in branches 1 and 2 before $q = 375$ cm^{-1} by arguments based on a usual but very sensitive phonon–polariton damping evolution as a function of q value. Figure 4 shows that below 375 cm^{-1} only the lowest dispersion branch can be detected. In contrast, near 375 cm^{-1}, the response of this lowest branch decreases, while the response from the two upper polariton branches appears. We demonstrate that these changes are related to a drastic modification of the damping rate around the polariton regime. In fact, as expected from temporal damping measurements (figure 5, left), and checked by equation (5) (figure 5, right) damping of the phonons of the lowest branch, to which number 1 refers in figure 5, increases rapidly around $q = 400$ cm^{-1}. It is due to a change of polariton regime from photon-like to phonon-like. Therefore, its contribution to the temporal domain signal decreases strongly from small time delays. Conversely, branch 2 evidences a photon-like regime close to the same q value. Moreover the phonon-like regime depicted by branch 2 at larger q values exhibits a significantly smaller damping constant for γ_{TO_2} than for γ_{TO_1}. Thus TO_2 phonons still contribute to the signal at longer time delays and are therefore more easily detected than TO_1 phonons. Invoking only one dispersion curve for this sudden shift in frequency near 400 cm^{-1} could be explained by coupling to a symmetry-forbidden mode. This would be the case in two-phonon states as suggested by Raptis [4]. Theoretical models built to describe this particular coupling rely on the Ω dependent γ parameter [13]. As previously noticed [6], it predicts small dispersion changes for the phonon–polariton frequency, but would lead to drastic modifications of the damping dispersion that we did not detect. We have also represented in figure 4 a hypothetical splitting

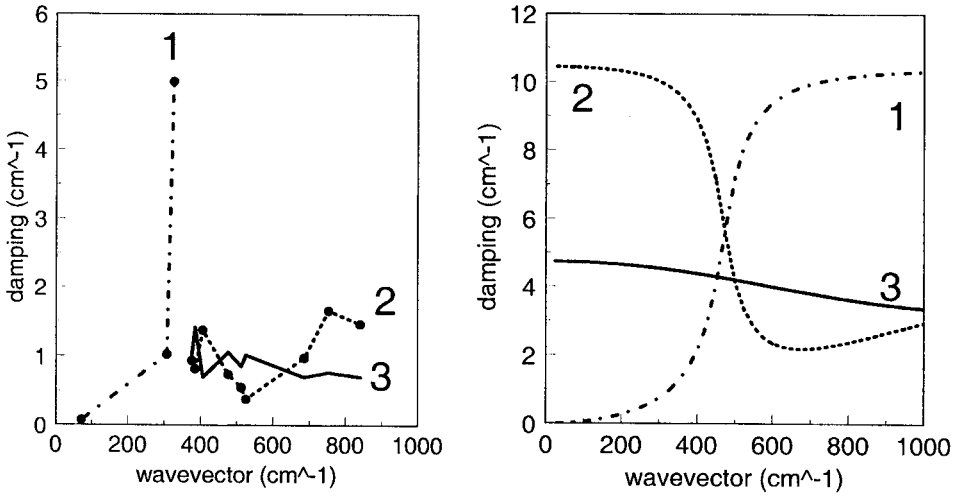

Figure 5. Left: evolution of the damping deduced from the three lowest phonon–polariton branches, using equation (2) for fitting the temporal domain results; right: evolution of the damping of the polariton as expected from equation (5); curves are labelled 1 to 3 in agreement with figure 4.

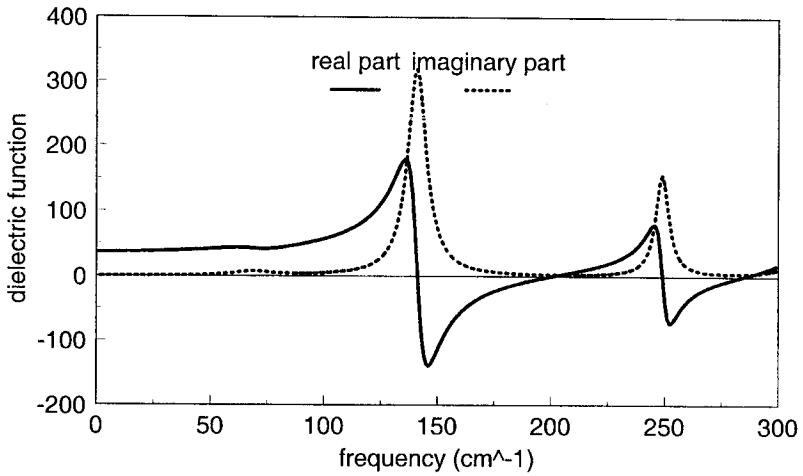

Figure 6. Real and imaginary dielectric function as calculated from equation (4), using parameters of table 2 and with $\varepsilon_{\perp}(\infty) = 4.82$.

of the third dispersion curve. Nevertheless, the accuracy of our actual set-up does not allow us to draw conclusions in that case; moreover, the changes in oscillator strengths given in table 2 by numbers in parentheses are negligible.

Fitting the dispersion curves gives an estimate of the oscillator strengths. They have been used to calculate the real and imaginary parts of the dielectric constant in this frequency region (figure 6), paying attention that the calculated curves take only into account the phonon contribution to $\varepsilon(\omega)$. In fact, they should be confronted with experimental results performed in the infrared spectral region to estimate the contribution of Debye relaxational modes [2] to the dielectric constant. We notice that the predicted two main peaks correspond to infrared data by Johnston [1], with a comparable oscillator strength ratio.

Having examined the phonon behaviour in a q sensitive range, we can draw conclusions with confidence on the three lowest TO and LO values from E-symmetry modes in $LiTaO_3$ and on their associated dispersion curves. This work demonstrates the ability of femtosecond pulses to easily excite and detect phonons in the polariton regime. The use of shorter pulses would allow us to reach higher lying branches that are not accessible using our existing set-up. A more extensive work in the temporal domain is planned to investigate the signal intensity evolution as a function of q. It would permit us to compare directly A_j and s_j parameters and have therefore a better insight into ionic and electronic contributions to electro-optical parameters.

The study of $\omega = f(q)$ dispersion curves for E-symmetry polaritons has allowed us to analyse the $\varepsilon_\perp$ component of the dielectric tensor. This is the counterpart of the study of A_1-symmetry polaritons [5] which led to the $\varepsilon_\parallel$ component [9].

References

[1] Kaminov I P and Johnston W D 1967 *Phys. Rev.* **160** 519
Johnston W D and Kaminov I P 1968 *Phys. Rev.* **168** 1048
Johnston W D 1970 *Phys. Rev.* B **1** 3494
[2] Penna A F, Chaves A, Andrade P da R and Porto S P S 1976 *Phys. Rev.* B **13** 4907
Penna A F, Chaves A and Porto S P S 1976 *Solid State Commun.* **19** 491
[3] Yang X, Lan G and Wang H 1987 *Phys. Status Solidi* b **141** 287
[4] Raptis C 1988 *Phys. Rev.* B **38** 10 007
[5] Bakker H J, Hunsche S and Kurz H 1993 *Phys. Rev.* B **48** 13 524
[6] Wiederrecht G P, Dougherty T P, Dhar L, Nelson K A, Leaird D E and Weiner A M 1993 *Ferroelectrics* **150** 103
[7] For a review, see Merlin R 1997 *Solid State Commun.* **102** 207
[8] Gautier C A, Loulergue J C and Etchepare J 1996 *Solid State Commun.* **100** 133
[9] Claus R, Merten L and Brandmuller J 1975 *Light Scattering by Phonon Polaritons (Springer Tracts in Modern Physics)* (Berlin: Springer)
[10] Albert O, Duijser M, Loulergue J C and Etchepare J 1996 *J. Opt. Soc. Amer.* B **13** 29
[11] Bond W L 1965 *J. Appl. Phys.* **36** 1674
[12] Barker A S and Loudon R 1972 *Rev. Mod. Phys.* **44** 18
[13] Barker A S Jr 1968 *Phys. Rev.* **165** 917